Available on CMS information server

CMS NOTE 1999/032

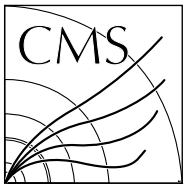

The Compact Muon Solenoid Experiment

CMS Note

Mailing address: CMS CERN, CH-1211 GENEVA 23, Switzerland

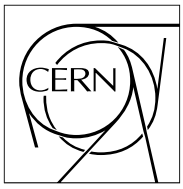

Dec 21, 1998

THE OPERATION OF VACUUM PHOTOTRIODES IN A NON-AXIAL MAGNETIC FIELD - A MONTE-CARLO STUDY

J.E.Bateman

Rutherford Appelton Laboratory, Chilton, Didcot, Oxon, UK.

Abstract

The predictions of a simple monte-carlo model of the operation of vacuum photo-triodes in a non-axial magnetic field are presented and compared to some available experimental measurements.

1. Introduction

In a previous report [1] the predictions of a simple monte-carlo model of the operation of a typical vacuum phototriode (VPT) in an axial magnetic field were shown to reproduce the observed behaviour of the experimental devices tested. In particular the dependence of the magnetic hardness of the electron gain and the excess noise factor on the detailed design of the VPT was explained in terms of the model. In the CMS ECAL endcap the VPT axes will in general be aligned at an angle lying between roughly 10^o and 25^o to the solenoid magnetic field (4T). The present report describes a modified version of the monte-carlo model which permits the simulation of VPT operation when the electric field (**E**) and the magnetic field (**B**) within the drift sections of the VPT (figure 1) do not coincide in direction. The surface interaction modelling is preserved as described in [1] and the kinematics of the electron motion in the cathode-anode and anode-dynode gaps are modified to take account of the finite angle (θ) between **E** and **B.**

The finite value of θ introduces a geometric distortion which leads to electrons from one electrode missing the target electrode as they tend to follow the magnetic field rather than the electric field. This requires that the model take account of the finite width of the electrode system. In the model (for convenience) the electrodes are considered as square and of edge dimension 20mm. As in the previous version of the model **E** and **B** are required to be constant in magnitude and direction over the active aperture. Neither the inevitable distortions of E at the edge of the active area nor any local distortion in **B** can be modelled. As before [1] the electric field is treated a being constant in each of the electrode gaps.

The finite value of θ also invokes effects from the symmetry of the mesh pattern on the anode. A rectangular mesh is assumed and the gain (G) and excess noise factor (F) are modelled as a function of the angle of the mesh pattern as it is rotated about the axis of the VPT (ϕ).

2. Electron motion in crossed electric and magnetic fields

The motion of an electron in combined electric and magnetic fields is given by the Lorentz equation:

$$m\mathbf{a} = e\mathbf{E} + e\,\mathbf{v} \times \mathbf{B}$$

where m and e are the mass and charge on the electron and **a** and **v** are its acceleration and velocity. This vector equation leads to a set of coupled differential equations which can be put into a tractable form by careful selection of the coordinate system. If one arranges for B to lie along a principal axis (x) as shown in figure 2 the equations of motion become:

$$\frac{d^2x}{dt^2} = \frac{e}{m} E\cos\theta \qquad (1)$$

$$\frac{d^2y}{dt^2} = \frac{e}{m}\left(E\sin\theta + B\frac{dz}{dt} \right) \qquad (2)$$

$$\frac{d^2z}{dt^2} = -\frac{e}{m} B\frac{dy}{dt} \qquad (3)$$

Integrating these equations with the initial conditions $\mathbf{x} = \mathbf{x_0}$ and $\mathbf{v} = \mathbf{v_0}$ at t=0 we obtain:

$$x = \frac{1}{2}\frac{\omega E}{B}\cos\theta\, t^2 + v_{0x}t + x_0 \qquad (4)$$

$$y = \frac{v_{0y}}{\omega}\sin\omega t - \frac{\beta}{\omega}\cos\omega t + y_0 + \frac{\beta}{\omega} \qquad (5)$$

$$z = \frac{\beta}{\omega}\sin\omega t + \frac{v_{0y}}{\omega}\cos\omega t - \frac{E}{B}\sin\theta\, t + z_0 - \frac{v_{0y}}{\omega} \qquad (6)$$

where:

$$\omega = \frac{Be}{m} \qquad \text{(cyclotron frequency)}$$

$$\beta = v_{0z} + \frac{E}{B}\sin\theta$$

In order to return to the coordinates (**x'**) of the VPT the following transform is used:

$$x' = x\cos\theta + y\sin\theta$$

$$y' = -x\sin\theta + y\cos\theta$$

$$z' = z$$

Considering the motion described by equations (4)-(6) it is quickly obvious that the electron motion is a spiral consisting of circular motion in the y,z plane with angular frequency ω and radius of curvature ρ where:

$$\rho^2 = (v_{0y}/\omega)^2 + (\beta/\omega)^2$$

while the centre of this orbit (y_c,z_c) drifts in the y,z plane, described by:

$$y_c = y_0 + v_{0z}/\omega + E\sin\theta/B\omega$$

$$z_c = z_0 - v_{0y}/\omega - E\sin\theta\, t / B \qquad (7)$$

The motion in the direction of B is simply uniformly accelerated motion:

$$x = \frac{1}{2}\frac{eE}{m}\cos\theta\, t^2 + v_{0x}\, t + x_0 \qquad (8)$$

The above analysis indicates that the simple tracking of electrons performed in the axial field case is also possible in the crossed field situation. Calculating the flight time of the electron across a gap using equation (4) permits the position and velocity at the next electrode to be evaluated from equations (5) and (6). Using the final values for one gap as the initial values for the next one permits the continuous tracking of an electron through the structure.

The main calculational penalty imposed is that frequent transforms must be carried out between the VPT and the B-defined axes. All interactions with surfaces must be calculated in the VPT axes and all motion in the B-defined axes. All the important surface interactions were preserved, only the backscattering on the anode mesh was omitted since this was found to have no observable effect on the results.

3. Simulation results

The design parameters from various experimental VPTs were inserted into the model and the gain and excess noise factor explored as a function of the angle between the VPT axis and the magnetic field θ (tilt angle) and the mesh rotation angle ϕ. If only θ is specified then the model was run with ϕ=0, i.e. the mesh pattern is parallel to the z axis. The VPT parameters required for the model are : cathode-anode spacing (d_{ac}), anode-dynode spacing (d_{ad}), anode mesh pattern frequency (L) in lines/mm and the anode mesh geometric transparency (T_r). The bias convention used is that the anode is at earth potential and the photocathode potential (V_c) and the dynode potential (V_d) are negative.The most complete set of data available of non-axial field measurements on VPTs is that presented by Dr Seliverstov at the June (‘98) CMS week on the RIE tubes. Accordingly the pararameters for the tubes tested have been put into the model. They are:

Tube	L (l/mm)	T_r
FEU-189-N56	30	0.67
FEU-189-N83	30	0.67
FEU-189-N105	60	0.49

All tubes have d_{ac} = 3.5 (±0.5)mm and d_{ad} = 2.0mm.

Data were also taken at RIE on the standard Hamamatsu tube type R2148 which has parameters: L=30.3l/mm, T_r=0.72, d_{ac}=4.5mm, d_{ad}=3.5mm.

3.1 Gain variation with θ and ϕ.

Figure 3a shows the model predictions for the dependence of the VPT gain for N83 (L=30l/mm, Tr=0.67) as a function of B (up to 4T) with the angle (θ) between **E** and **B** as a parameter and ϕ=0. Typically 5000 initial photoelectrons are used and this number determines the statistical noise in the results. Each point requires about 20 seconds of computer time (Pentium Pro 200 processor). The bias potentials are chosen to correspond with those used in the experimental tests

Figure 3b illustrates the model predictions for the VPT gain (N83) for the behaviour of the gain as a function of the field tilt angle (θ) at two specific values of the magnetic field (B=1.4T, B=4.0T). Again $\phi=0^o$.

The model can be used to explore the effect of the mesh frequency on the gain at a typical value of θ (20^o) as a function of the magnetic field. Figure 4 shows the model predictions for N83 (30l/mm) and N105(60l/mm).

For the examination of the interaction of θ and ϕ on the gain as a function of the magnetic field the parameters of the standard Hamamatsu tube R2148 were chosen (L=30.3l/mm, T_r=0.72, d_{ac}=4.5mm, d_{ad}=3.5mm, V_c=-1000V, V_d=-300V). Figure 5a shows the model results for the gain with θ fixed at the typical value of 20^o and ϕ varying from 0 to 40^o. Further runs with the model show that the curves are completely symmetrical about $\phi=45^o$. Figure 5b shows the model gain predictions as a function of the mesh angle (ϕ) at a fixed tilt angle ($\theta=30^o$) and magnetic field. The special B-field values of 1.5T and 2.0 T are chosen to highlight the effect of the gain dips observed between 1.2T and 2.0T seen in figure 5a. (These gain dips are due to resonant effects induced by the regular mesh structure as the electrons drift in the **E**x**B** direction, and are discussed in detail in Section 5.1.)

In order to simulate the practical situation in which the VPTs would be installed with no control of the mesh orientation Figure 6a presents the model gain as a function of θ with ϕ as a parameter at B=4.0T for tube N105. Figure 6b shows the same plot made with B=1.5T, i.e. in the middle of the resonance observed in figure 5a.

3.2 The Excess Noise Factor as a function of θ and ϕ.

The model was adapted to calculate the excess noise factor (F) from the single electron response function (SERF) as detailed in reference [1]. Figure 7a is a plot of the model predictions for F and the gain of R2148 (V_c=-1000V,V_d=-300V) at a typical range of θ and ϕ values. As observed before [1] F rises steadily with the magnetic field in all orientations. Increasing both angles improves the gain and F. The obvious anti-correlation between F and G in figure 7a suggested that the data be replotted with F as a function of G for two of the data sets. Figure 7b shows that a systematic correlation exists between F and G.

4.0 Comparison of the Model with Experimental Data.

4.1 RIE Data

4.11 Gain measurements

Figure 8a shows a comparison between the model predictions and the measured data on N105 for $\theta=0^o$ and figure 8b for $\theta=20^o$. Figure 9 shows the comparison of G as a function of θ at b=1.5T and 4.0T. While the trends of the model data and the experimental data broadly agree there is an obvious discrepancy. In the gain curves the experimental data show a precipitate decline at low (B<0.5T) magnetic field values, conforming more to the model at larger B values. Referring back to the comparison between the model and the experimental results from FEU-189-N37 in reference [1] we see that in the case of central illumination of the photocathode the experimental data reproduces the the initial concave-down portion of the G versus B curve seen in the model data of figure 8a. The precipitate initial decline seems to be a feature observed with full cathode illumination (an illumination diameter of 15mm was used in these tests), and the effect is proportionately worse as θ increases.

The discrepancy between centre-field and full-cathode illumination gain curves has already been noted in the context of the data provided in the Hamamatsu R2148 data sheet [1]. Figure 10 shows the two experimental curves (θ=0) along with the model data. The sharp loss of gain at low magnetic field values is particularly evident in full-field illumination. This behaviour could be interpreted as a loss of effective cathode area as a function of magnetic field which limits at a low B value. A model of such an effect can be made in the light of the following facts:

- The process of photocathode production produces an active area which extends (in general) across the whole inside face of the tube (and even down the walls slightly).

- Photoelectrons must pass through the active (transparent) part of the anode surface to reach the dynode and this area is (in general) several millimeters smaller in diameter than the tube bore.

- In zero (or low) magnetic fields the trajectories of photoelectrons are controlled by the electric field which can be sufficiently distorted transaxially to make use of an area of cathode larger than the anode mesh aperture.

- At quite modest B field values (0.2T) the magnetic field imposes its geometry on electron collection. In an axial magnetic field the useful photocathode area is limited to the anode mesh open aperture. In a tilted field the geometric mis-match leads to an increasing loss of photoelectrons as θ is increased (and the electrons hit the tube wall).

- Quite a modest (≈1mm) loss of active diameter will lead to a significant signal loss.

- Measuring the gain by dividing the anode current by the cathode current will reveal this effect as a gain deficit because the photoemission is not affected, only the transfer efficiency to the dynode.

Using these ideas a simple model can be made in which a dead border of cathode is assumed which grows rapidly with B to a saturation value (when the electron transfer geometry is defined entirely by the B field). The simplest form of function suitable to describe the width of the dead border is $\delta x = \delta x_{max}(1-e^{-B/Bs})$ where B_s is a scaling magnetic field value. The correction factor to the gain for an active diameter of D is thus approximately $(1- \delta x/D)^2$. Turning to the data in figure 10 it is seen that multiplying the model data by this factor with δx = 3mm, D=20mm and B_s=0.05T gives a very plausible fit to the experimental data for full cathode illumination. In the case of a 14mm diameter active area the response also shows signs of a similar but weaker effect. This can be interpreted as due to the fact that unless the active area is very tightly constrained to be near the axis of the tube, light scattering in the thick photocathode window and reflection of transmitted light from the reflective interior components is capable of reaching the extended cathode edges. In the absence of a magnetic field, the electric field will allow collection of the photoelectrons thus generated which will add a small fraction to the total signal. In the presence of a sufficiently high magnetic field these additional electrons will not reach the active central region of the VPT. The model will see this loss of signal on switching on the B field as a small effective dead border, evaluated in this case as 0.3mm.

Incorporating this model into the monte carlo data for N105 in the cases of $\theta = 0$ (figure 11) and $\theta = 20^o$ (figure 12) permits the form of the experimental gain versus B curves to be modelled more accurately. There is, of course, no reason to expect perfect agreement from the arbitrarily chosen function for the B-dependence of the dead border - the function required clearly differs slightly in the two cases in figures 11 and 12. As anticipated, the geometric mis-match forced by the angled B field makes δx_{max} twice as large (3mm) in the case of $\theta = 20^o$ as in the axial field case (1.5mm).

A plausible geometrical model can be made to take account of the θ behaviour of the dead border. However, it all becomes rather *ad hoc* and really requires modelling of the E field around the cathode edges which is beyond the scope of the present model. The discrepancy between the model and the experimental data in the gain versus θ plot at B=4T (figure 9) is now explained by the dependence of δx_{max} on θ and the model data can be corrected down to match the experimental data at higher values of θ.

4.12 Excess noise measurements.

Comparing the model behaviour of the excess noise factor (F) as a function of B with the experimental data for FEU-180-N56 (figure 13) shows general agreement but detailed disagreement. The dead border effect will, inevitably, have some effect on the measured F value, but this is difficult to estimate, except to say that the sharp drop in gain at low B values should (by figure 7b) give rise to an initial rise of F with B. The value of F predicted at at B=4.0T is in the region of 2.5 at $\theta = 20^o$ in reasonable agreement with the measurements.

4.2 Brunel Data

Figure 14 compares the predictions of the variation of the gain (relative to the B=0 case) as a function of the tilt angle with the data recorded at Brunel on the tube E/T 10,001 at B=4.7T. As with previous experimental data sets, the agreement is good on the general level and trend of the effects but poor in detail. The different bias conditions tested invoke second order effects (dependent on local non-uniformity of the electric field) which the model does not handle.

Note that for these tests the VPT bias arrangements made the anode and dynode positive with respect to the earthed cathode.

5. Discussion

5.1 The effect of tilt angle on the VPT gain

In the previous report [1] it was demonstrated that the decrease of gain observed in a VPT as the axial magnetic field increases is due to the fact that the electron motion becomes increasingly constrained by the magnetic field which keeps secondary electrons focussed in the centres of anode mesh gaps and unable to hit the anode and generate an output signal. Imposing a finite angle (θ) between the electric and magnetic fields generates the motion described in section 2 above, which is very similar to the motion in an axial **B**-field but shows (in addition to the orbital motion) a drift in the z direction (analogous to a Hall drift in a semiconductor).

As equation (7) shows this is a constant drift velocity $v_{cz} = E\sin\theta/B$. Inserting typical values into this formula shows that, at typical operating conditions and $\theta \approx 20^o$, this gives rise to a shift δz of the order of tens of microns. In the case of a fairly fine mesh this is more than enough to overcome the focussing effect of the axial component of B and give the secondary electrons more oportunities to strike a bar of the anode mesh and so enhancing the gain. Figure 3a shows that the model predicts a very useful improvement in the magnetic hardness of FEU-189 N83 as the tilt angle is increased.

Above $\theta = 20^o$ (figure 3a) the gain response shows repeated gain dips as a function of B (e.g. at B≈1.0T and B≈2.0T at $\theta = 35^o$). This is not surprising - the mesh is a regular structure and when $\delta z = 1/L$ the electrons again go down the middle of the mesh holes and cause a dip in the gain. Thus we can expect resonant dips at B_{res}, where:

$$B_{res} = E\sin\theta t'/\lambda$$

where $\lambda = 1/L$ (mesh cell width) and t' is the transit time of the electrons in the gap concerned which can be obtained from equation (8) if one neglects any initial electron velocity:

$$t'^2 = \frac{2d^2 m}{eV\cos\theta}$$

where d and V are the gap width and potential difference.

Substituting for t' gives:

$$B_{res} = (2Vm/e\lambda^2)^{1/2} \sin\theta/(\cos\theta)^{1/2}$$

This relation implies that a plot of the measured dip positions from figure 3a against $\sin\theta/(\cos\theta)^{1/2}$ should result in a straight line fit. Choosing the dip features with the higher B values (they are better defined than the lower dips) gives three points $\theta = 20^o$, B=1.0T, $\theta=30^o$, B=1.7T, $\theta=35^o$, B=2.0T, which give a straight line fit with a slope of 3.59. Evaluating the slopes predicted by the above equation gives values of 3.03 for the anode-cathode gap and 1.43 for the anode-dynode gap. The gain curves at $\theta=30^o$ and $\theta=35^o$ clearly show two dips approximately a factor of two apart in B (e.g. B=1.0T and B=2.0T at $\theta=35^o$) which would seem to correspond to the resonant effects in the anode-dynode gap (lower dip) and cathode-anode gap (upper dip).

As figures 3a and 3b show, there is a region of B,θ parameter space in which the gain can be quite erratic in its behaviour due to the resonances described above (B<2T and $\theta>20^o$). At B=4T these effects are neglible up to the highest tilt angles relevant to the Endcap design.

All other things being equal one would expect a tube with finer mesh to perform better than one with coarser mesh. Figure 4 shows that the magnetic hardness for a device with L=60l/mm is indeed better than that of one with L=30l/mm. However, the "Hall" drift is sufficiently large for the advantage to be small at tilt angles in our range.

Since the "Hall" drift is highly directionally defined, it is inevitable that rotation of the mesh pattern about the VPT axis will modulate the gain. As figure 5a shows, the effects are strongest at B values around the main resonance (B=1.4T). Unsurprisingly, the curves of figure 5a are found to be perfectly symmetric about $\phi=45^o$. At B=4T a small advantage is predicted (+15%) for the optimum of $\phi=45^o$. Figure 5b shows the much more controlled behaviour of the gain with ϕ at B=4T compared with the behaviour in the region of the resonance.

Figure 6a shows the model predictions for the sensitivity of the gain to ϕ as a function of the tilt angle (θ) at B=4T. Basically the effect only switches on at the top of the angular range of interest to the Endcap. At $\theta=25^o$ a 20% modulation of the gain is predicted.

5.2 The effect on the Excess Noise Factor

As figure 7a shows, according to the model, the excess noise factor (F) is improved considerably at high B fields by introducing a tilt angle (θ) of 20^o. Rotating the VPT to the optimum angle of 40^o (ϕ) produces a further smaller improvent in F. Since no fundamental change in the electron transport mechanisms result from the rotations it is likely that the modulation of F results directly from the modulation of the gain.

The studies of the single electron response functions (SERF) in reference [1] indicated that the low gain observed at higher B fields was characterised in the SERF by a strong increase in the numbers of single electron events which had either one or very few secondary electrons. Thus an anti-correlation of G and F is inevitable.

Figure 7b shows the relation between G and F for sets of model data at $\theta=0^o$ and $\theta=20^o$. A relation of the form $F = b + a/G^4$ is observed in both cases. While F is lower for the angled case at high B field, this is because the gain is higher. The $\theta=20^o$ curve always lies above the $\theta=0^o$ curve. This is no doubt a consequence of the loss of photoelectrons caused by the geometric cathode-anode mismatch as θ increases. However, the generally higher level of the gain at high B fields more than compensates.

In a practical VPT the possibility of deadening the outer edge of the photocathode (as outlined in section 4.11 above) can lead to a further loss of gain (and thus an increase in F) as B increases up to around 1T. The experimental data in figure 13 shows a behaviour like this. While the detailed behaviour of the model and the experimental data are in poor agreement (probably for the same reason as the gain curves) again the magnitude of F (=2.5) is in close agreement at B=4T.

6. Conclusions

The “Hall” drift induced in the electron orbits in a VPT held at a finite tilt angle in a magnetic field partially compensates for the focussing effect of the B field which causes gain degradation in an axial field and results in a considerable increase in the magnetic hardness of the gain (and the excess noise factor) at B=4T. Some of this benefit is lost due to the geometric mis-match between the photocathode and the active anode aperture as θ is increased but according to the model there is an overall improvement.

In the measured data from RIE (and the Hamamatsu data sheet) it is appears that a further effect is in evidence when the whole cathode area is exposed. This effect leads to a considerable (20%) gain loss at low B fields (<0.5T) (see for example figure 8b) after which the gain is as flat as that predicted by the model. If the model for this effect proposed in 4.11 above is correct, then the gain contribution at B=0 arises from auxiliary peripheral areas of photocathode which are cut off by a value of B>0.5T. If the photocathode were physically matched in area to the anode, the gain at B=0 would be lower but the relative gain curve would (at $\theta=20^o$) be essentially flat.

A finite value of θ inevitably introduces a weak dependence of the gain on the angle of the mesh relative to the “Hall” drift direction. The model shows that at B=4T this is

negligible at small θ but can reach a magnitude of 20% at $\theta=30^o$. The optimum angle for the mesh angle is 45^o, and if it is not difficult to index this during manufacture, a small gain in G, F and the gain uniformity can be made.

As figure 7b shows, the excess noise factor is closely related to the gain of a tube. This is useful to know since, in general, G is easy to measure and F difficult to measure.

According to the model, a fine mesh tube will show superior magnetic hardness to a coarser one. Modelling the E/T 10,001 tube which has L=15.7 agrees with the Brunel data in predicting a relative gain of 0.5 at $\theta=20^o$ and B=4.7T. For tubes with L=30l/mm the relative gain is found to be ≈0.75 (figure 4) for the model and 0.6 from the RIE data (FEU-189 N83); with L=60l/mm the corresponding figures rise to 1.0 for the model and 0.62 from the experimental measurement (FEU-189 N105). Thus there would seem to be little benefit in going beyond L=30l/mm. (If the 20% gain drop at low B values could be eliminated the RIE experimental measurements would agree quite well with the model.)
While the model described in this and the previous report [1] seems to reproduce quite well the essential characteristics of VPT operation in a magnetic field there are clearly limitations to the degree of detailed agreement which can be expected when comparison is made with practical measurements. The detailed discrepancies noted above can be understood in terms of the following considerations:

- The model assumes a constant E field in each gap. The problem of the E field configuration between the photocathode and the anode has already been discussed. A similar problem arises at the anode mesh, where, over a short distance (about two mesh pitches) the fields are very distorted. Fine control of the gain by V_{ad} will not be reproduced by the model.

- The tolerances on all parameters are arbitrarily small in a mathematical model. Manufacturing tolerances in the tube and non-uniformity of the B field will tend to wash out dynamical effects. For example, the effect on the gain of the angled field are, in general, weaker in practice than in prediction. Much of this may be due to the inevitable geometric fluctuations in an etched mesh pattern. The resonant effect seen in figure 3a is only weakly suggested in the experimental data for FEU-189 N83.

Programing a model to incorporate all such detail would involve a level of effort that would be unlikely to be justified by the results. The nature of the stochastic processes which govern the gain of the VPT are such that the control of the gain by the various parameters is relatively weak and the trend of dependence of the gain on each is made manifest by the simple model used. The general conclusions seem to be that optimum magnetic hardness of the gain (and the excess noise factor which tracks the gain) is favoured by using the finest mesh possible and by operating with a moderate magnetic field tilt angle. The model also indicates that a small benefit may be obtainable by arranging for the mesh pattern to be at an angle of 45^o to the **E** x **B** vector. The discrepancies between the model and the experimental results may be useful in pointing the way to possible improvements in the tube design.

REFERENCE

J E Bateman, The operation of vacuum phototriodes in an axial magnetic field - a montecarlo study, RAL-TR-1998-059, CMS Note 1998/059.

FIGURE CAPTIONS

1. A sketch of the structure of a VPT. The biassing convention used in the model is that V_c and V_d are negative with the anode at earth.

2. Schematic of the coordinate systems used in the model. The system (x,y,z) is such that the magnetic field **B** lies along x and the x,y plane coincides with the plane defined by **B** and the electric field **E**. The (x',y',z') system is similar with x' lying along the **E** vector. Z and z' are coincident and point out of the page. Mesh rotation (ϕ) is around the x' axis. The mesh pattern is parallel to y' and z' (unless rotated).

3. (a) Simulation by the model of the gain of FEU-189 N83 (L=30l/mm) as a function of the magnetic field and the tilt angle (θ).
(b) The relative gain predicted for FEU-189 N83 at B=1.4T and B=4.0T as a function of tilt angle (θ).

4. A comparison between the gain versus B curves predicted by the model for two tubes with differing meshes (L=30l/mm and L=60l/mm). The bias values are those used in the experimental tests.

5. (a) A plot of the simulated gain versus B curves with $\theta=20^o$ and ϕ varying between 0 and 40^o. The tube parameters are for the Hamamatsu R2148.
(b) The model predictions for the dependence of the gain on the mesh angle (ϕ) at $\theta=30^o$ and various magnetic field values.

6. (a) The modelling of the gain of FEU-189 N105 as a function of θ at B=4.0T showing the spread induced by the full range of possible mesh rotation angles.
(b) As before with B=1.5T.

7. (a) This plot shows the modelled response of the gain and the excess noise factor of R2148 to variation of θ and ϕ for a few relevant cases.
(b) Using the data of figure 7a the dependence of the excess noise factor on the gain is demonstrated.

8. (a) A comparison of the model gain data for FEU-189 N105 with the experimental measurements at $\theta=0^o$.
(b) The same comparison at $\theta=20^o$.

9. A comparison between the model and experimental data for the relative gain as a function of tilt angle for FEU-189 N105.

10. A comparison of the gain versus B (axial) curves from the Hamamatsu data sheet for the R2148 in the cases of centre cathode and full cathode illumination with the montecarlo model predictions, modified by the "dead cathode border" model.

11. A comparison between the gain predictions ($\theta=0^o$) for FEU-189 N105 and the experimental data with and without the "dead cathode border" model.

12. As for figure 11 with $\theta=20^{o}$.

13. A comparison between the model and experimental data for the excess noise factor of FEU-189 N56 at $\theta=0^{o}$ and $\theta=20^{o}$.

14. A comparison of the relative gain predicted for E/T 10,001 as a function of tilt angle (θ) at B=4.7T and the experimental data at various bias conditions. Note the different bias convention: cathode at earth, anode and dynode positive.

15. A fit of the B values of the (highest) resonant dip in the gain curves of figure 3a to the proposed model.

FIGURE 1

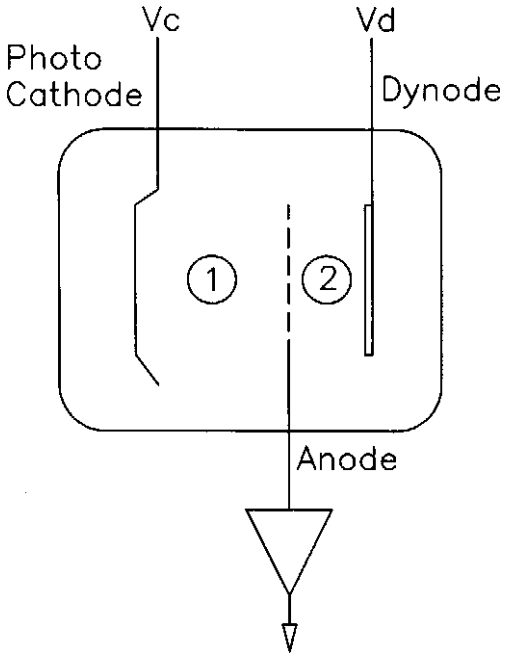

Typical Bias Conditions:

-1000V	0V	-300V
-900V	0V	-200V

FIGURE 2

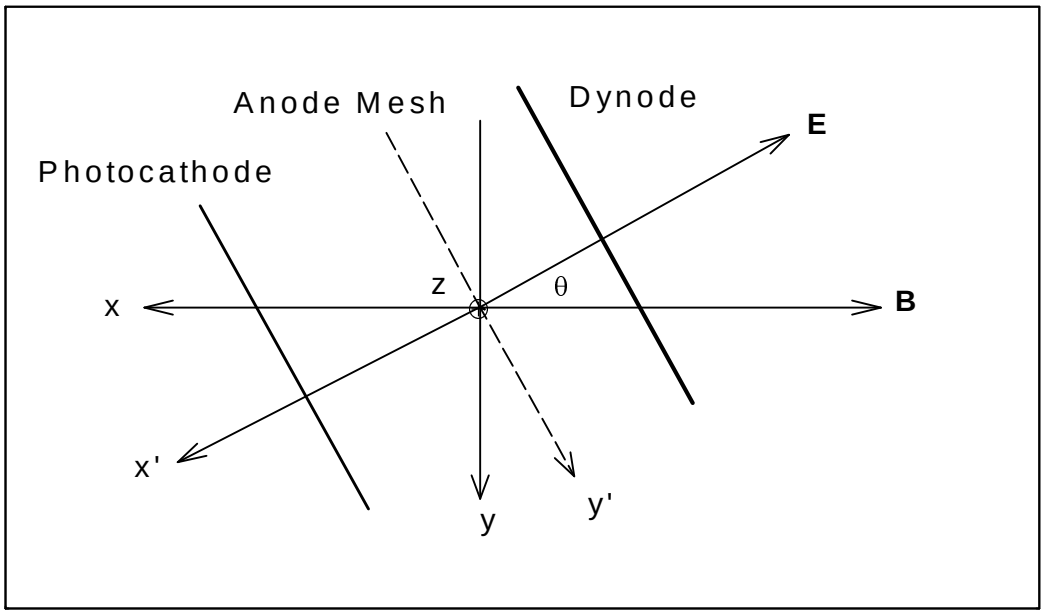

FIGURE 3a

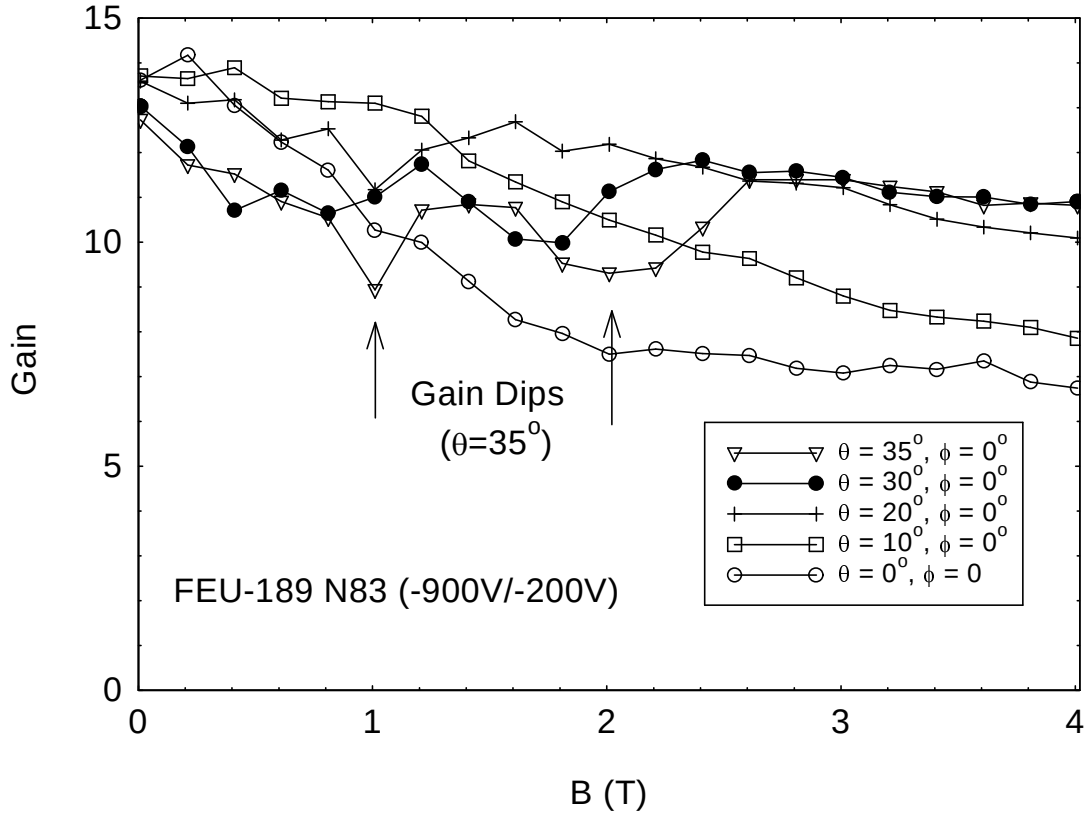

FIGURE 3b

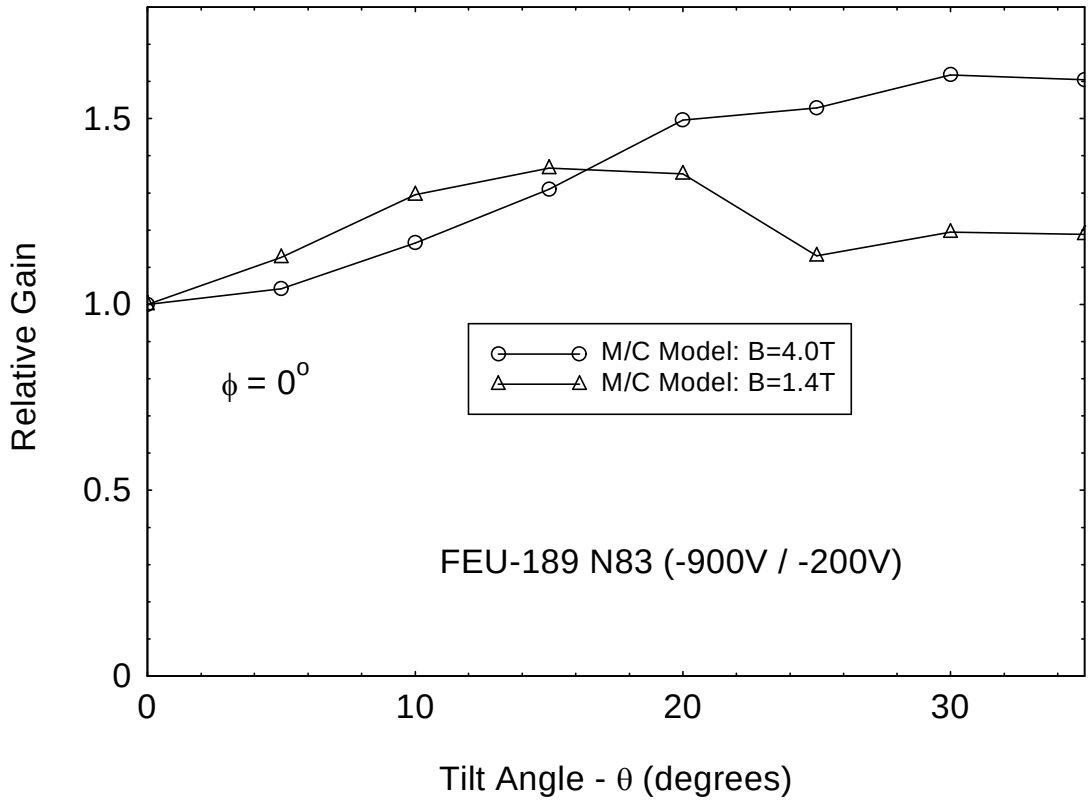

FIGURE 4

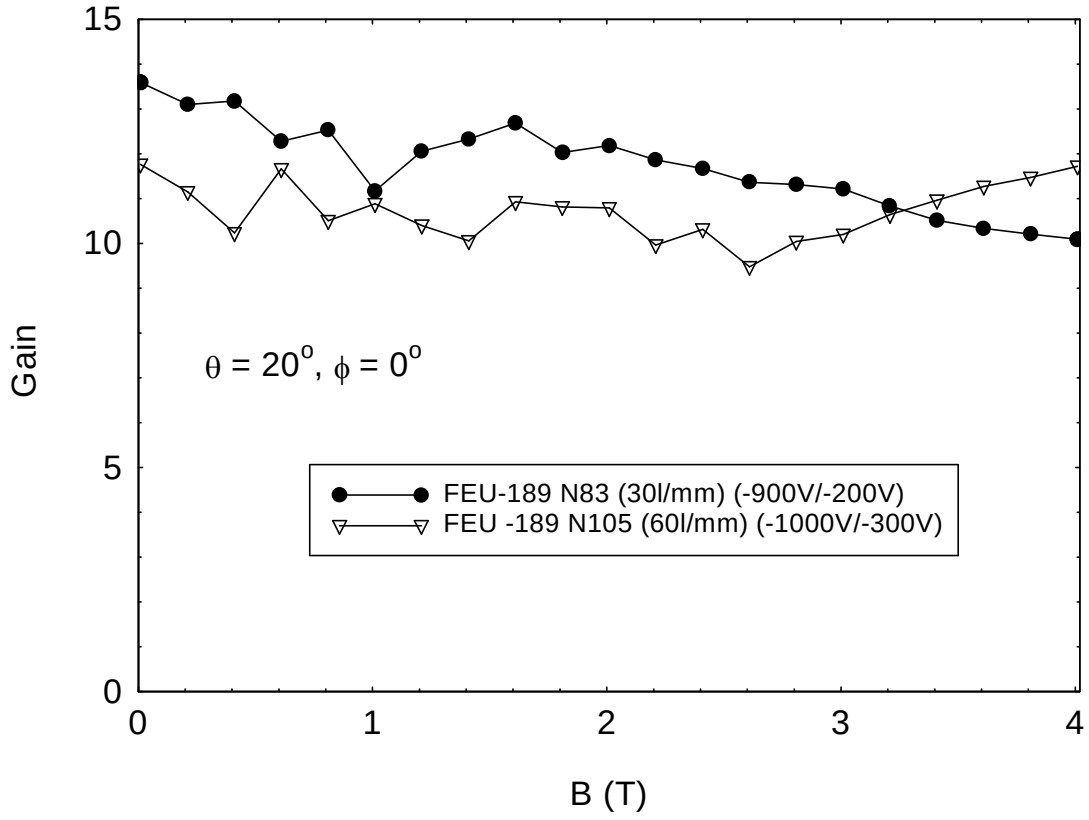
15
10
5
0
Gain
0
1
2
3
4
B (T)
θ = 20°, ϕ = 0°
FEU-189 N83 (30l/mm) (-900V/-200V)
FEU -189 N105 (60l/mm) (-1000V/-300V)

FIGURE 5a

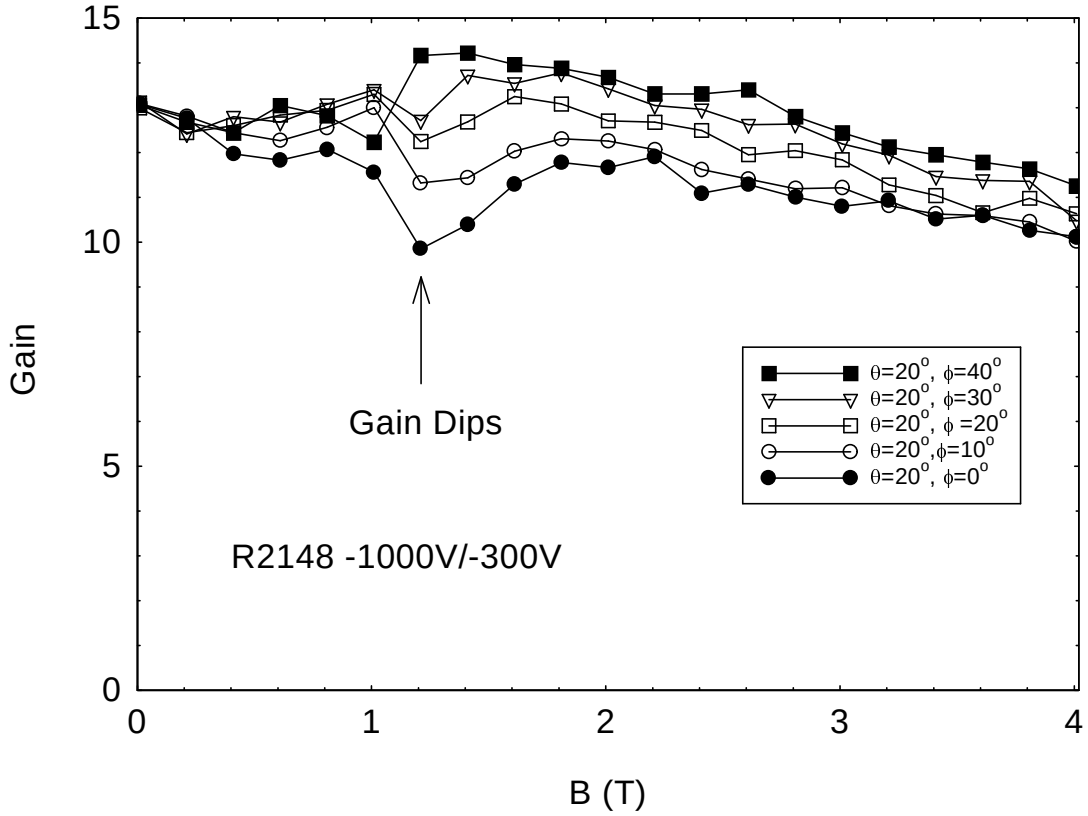

FIGURE 5b

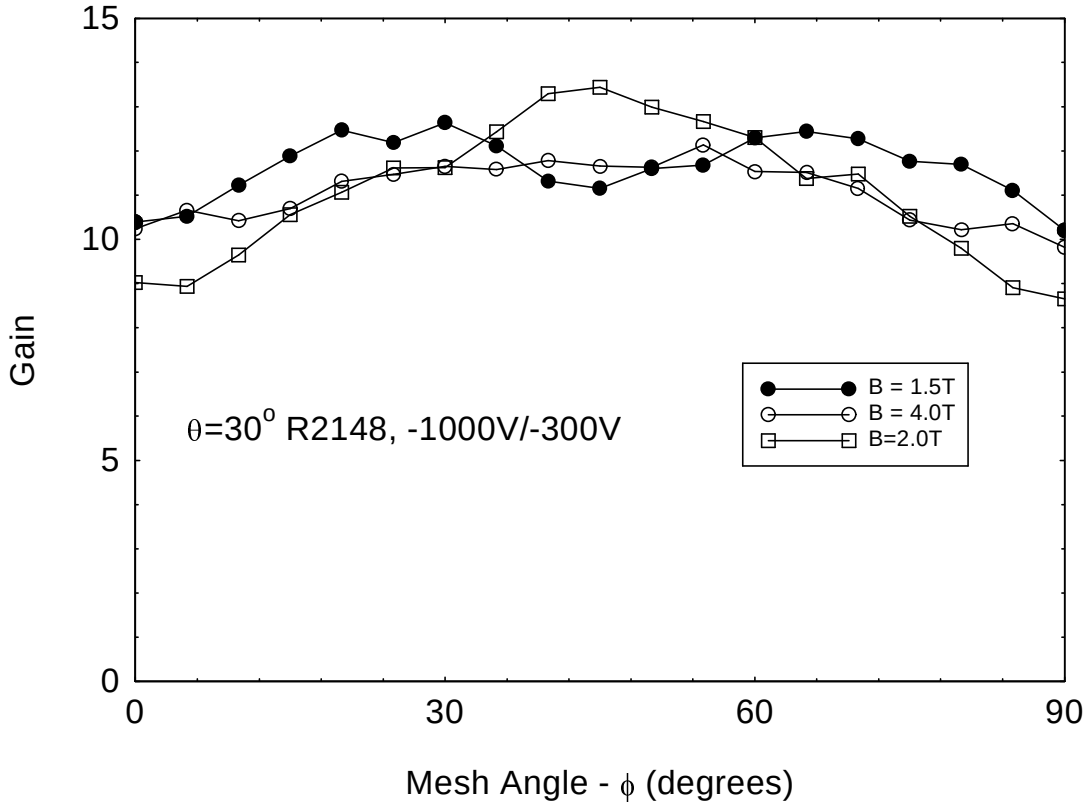

FIGURE 6a

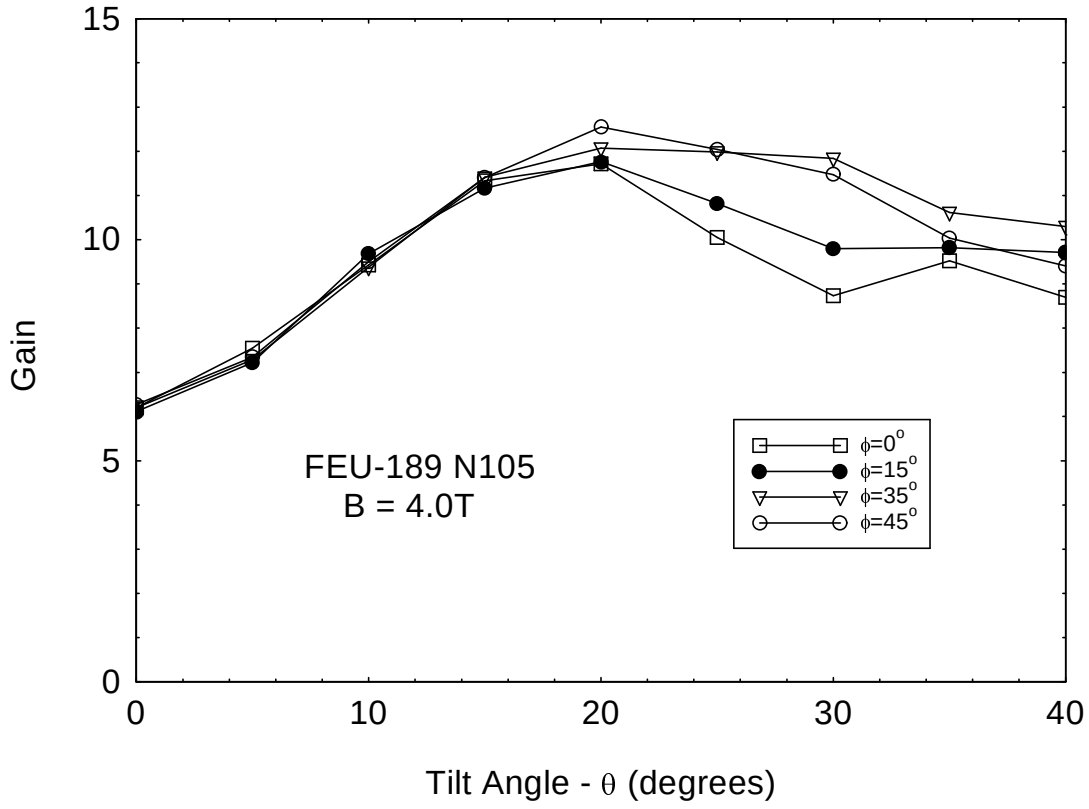

FIGURE 6b

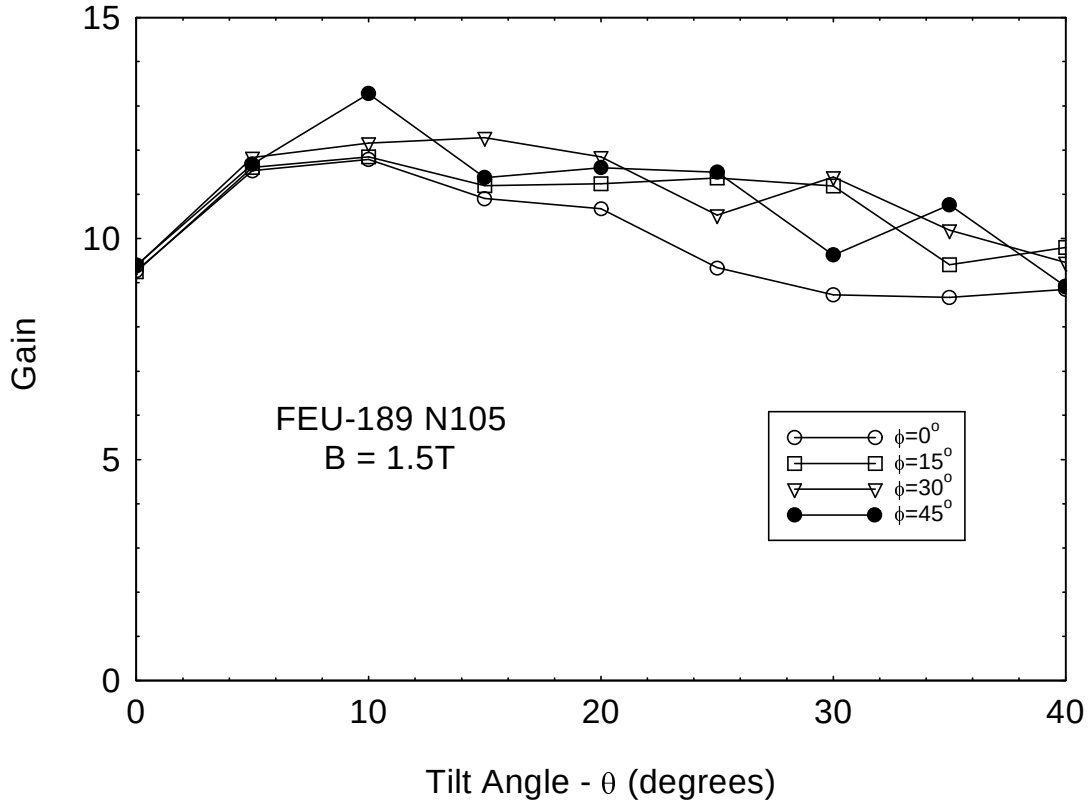

FIGURE 7a

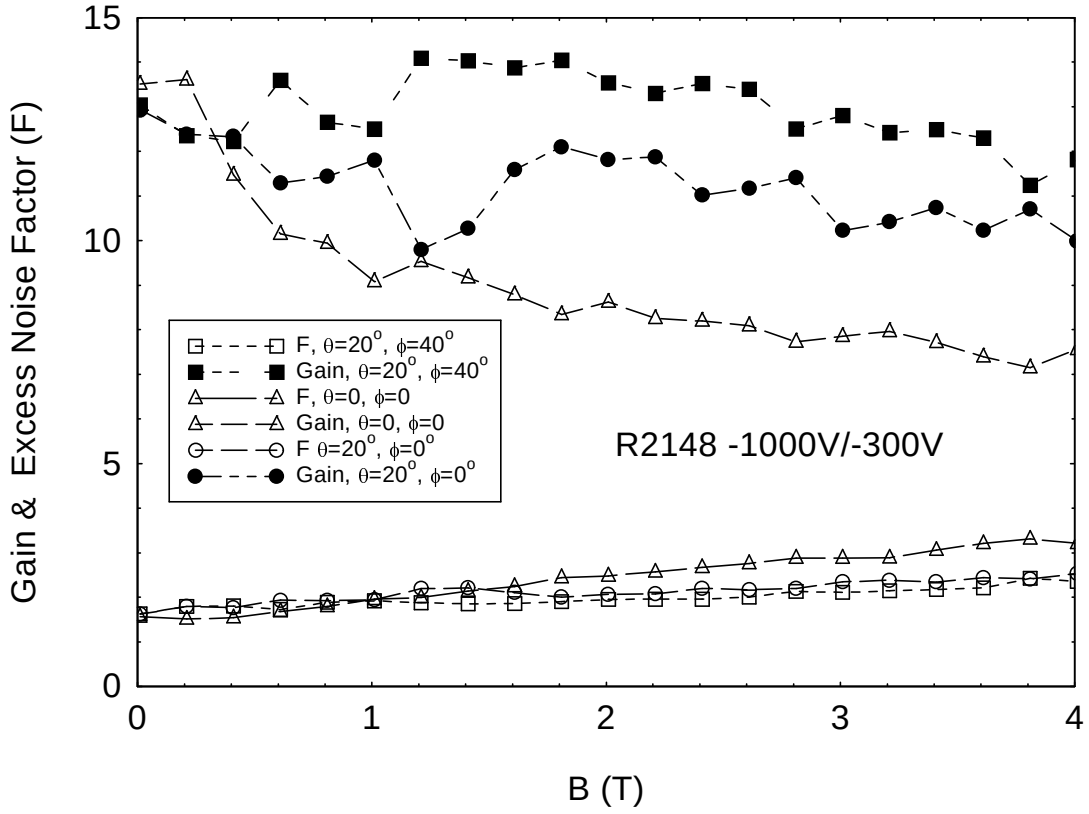

FIGURE 7b

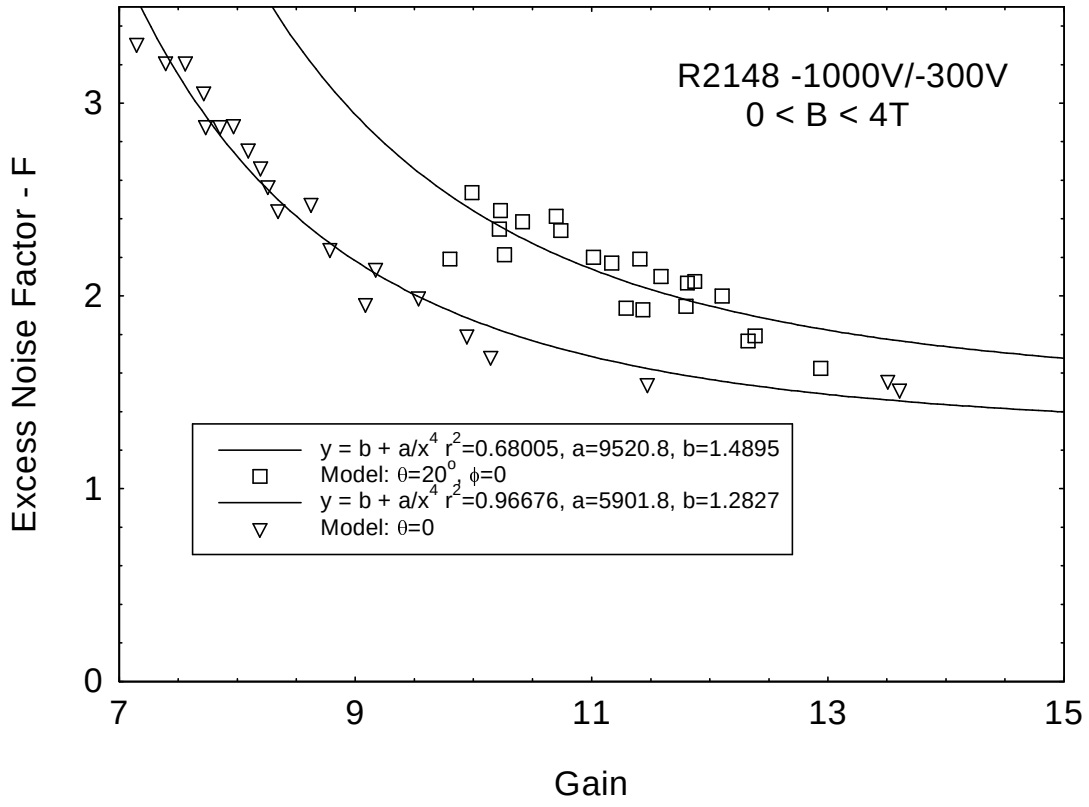

FIGURE 8a

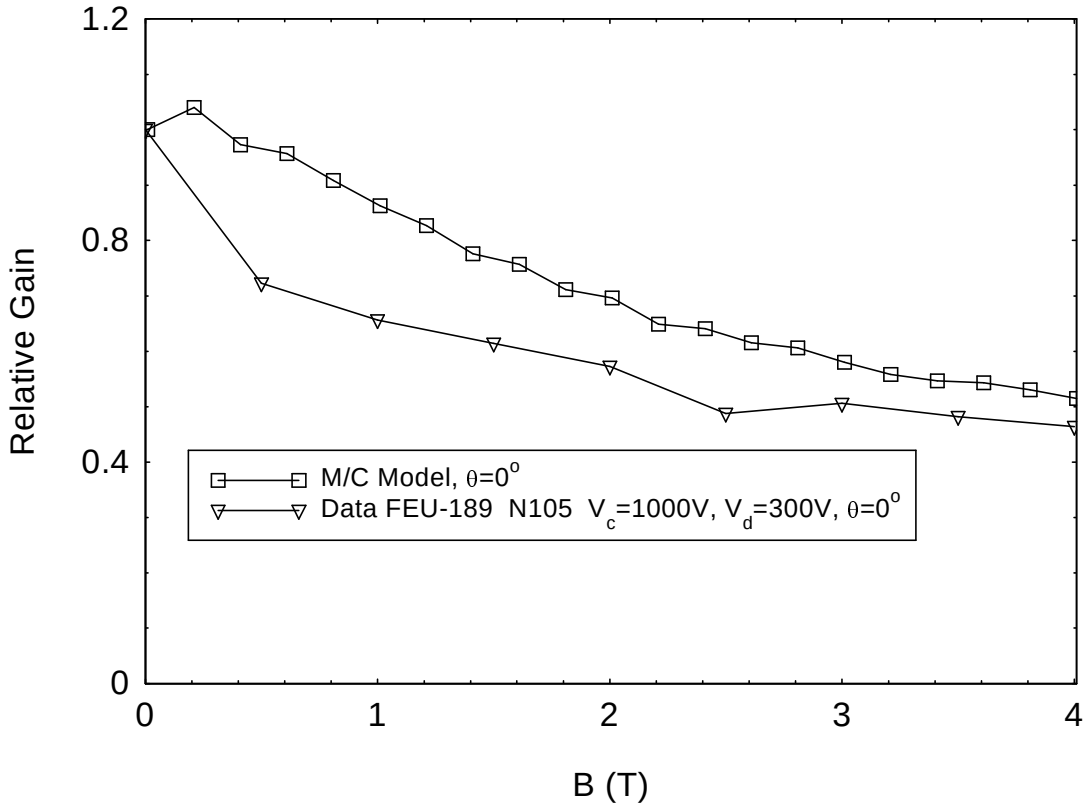

FIGURE 8b

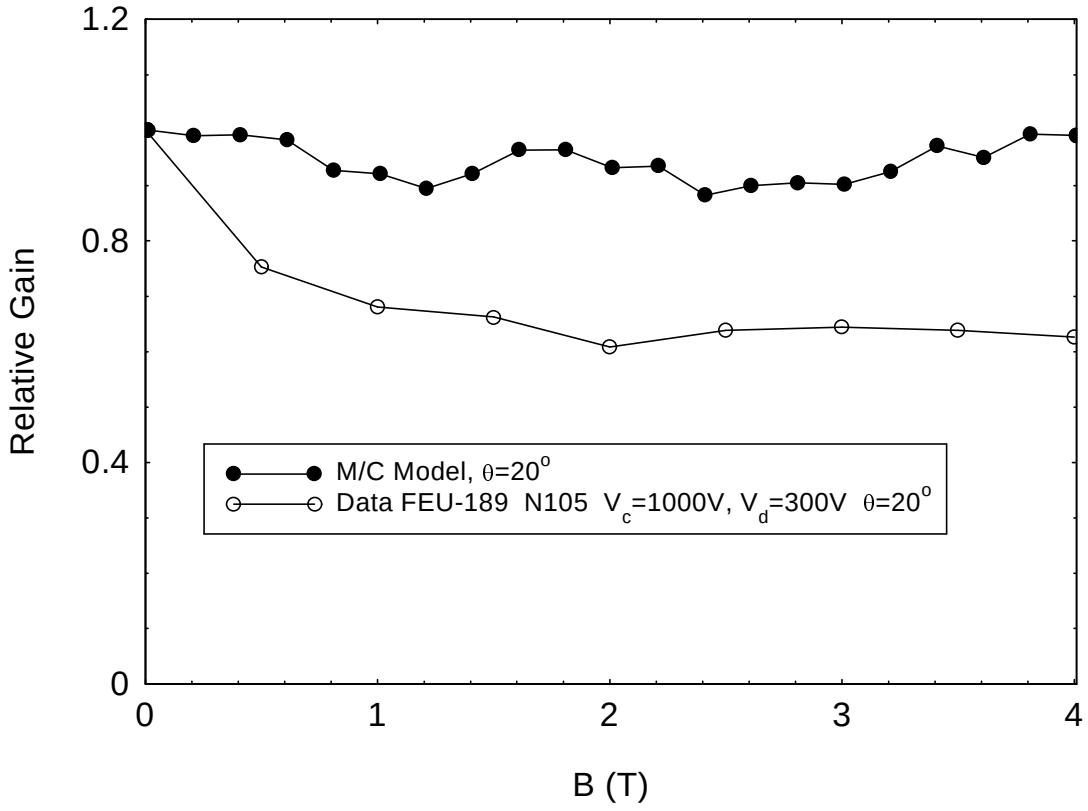

FIGURE 9

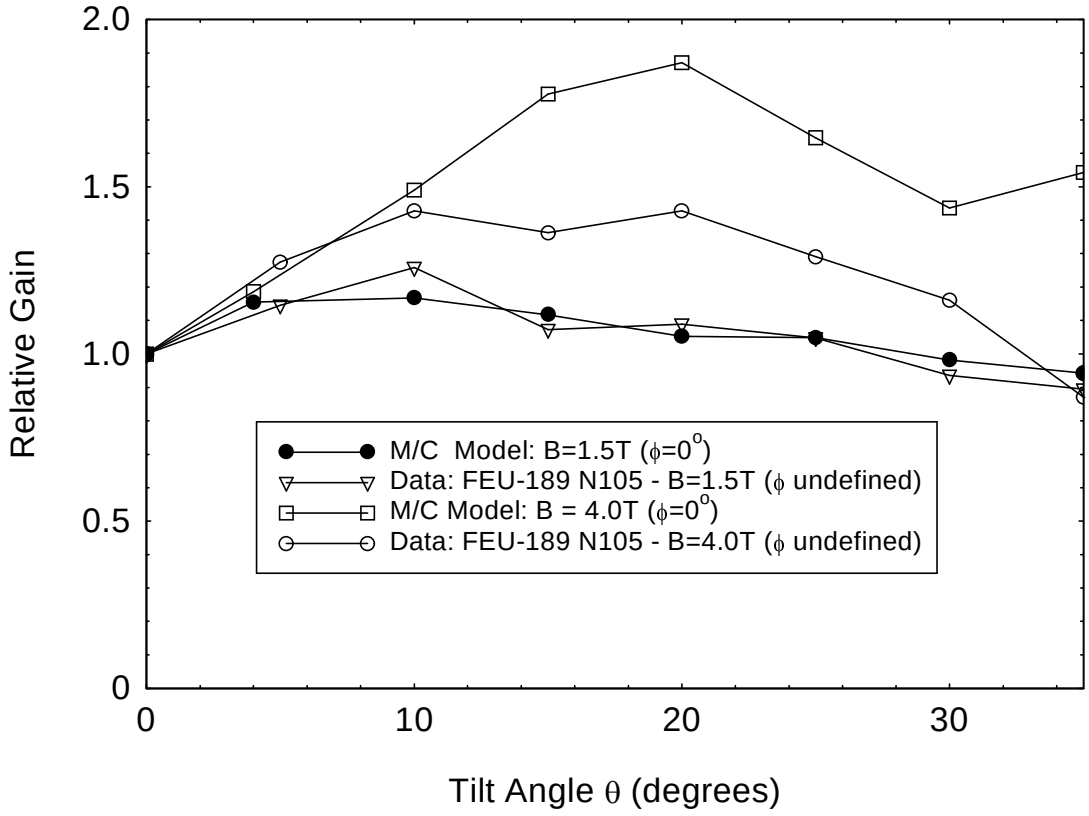

FIGURE 10

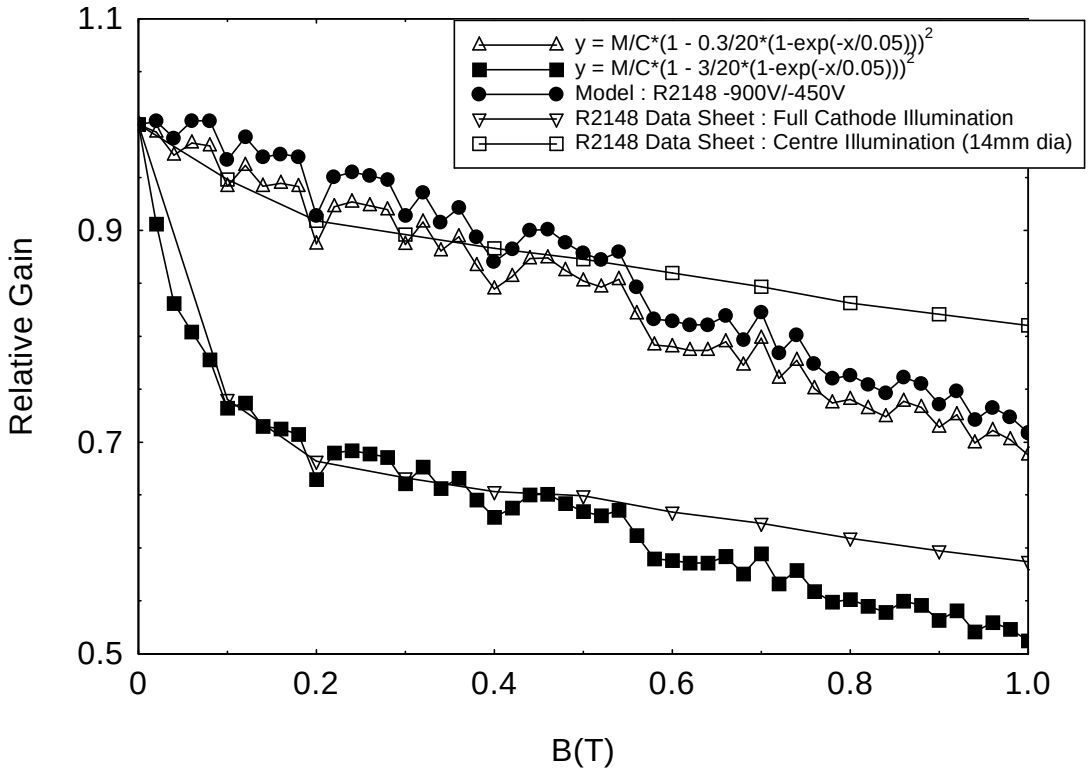

FIGURE 11

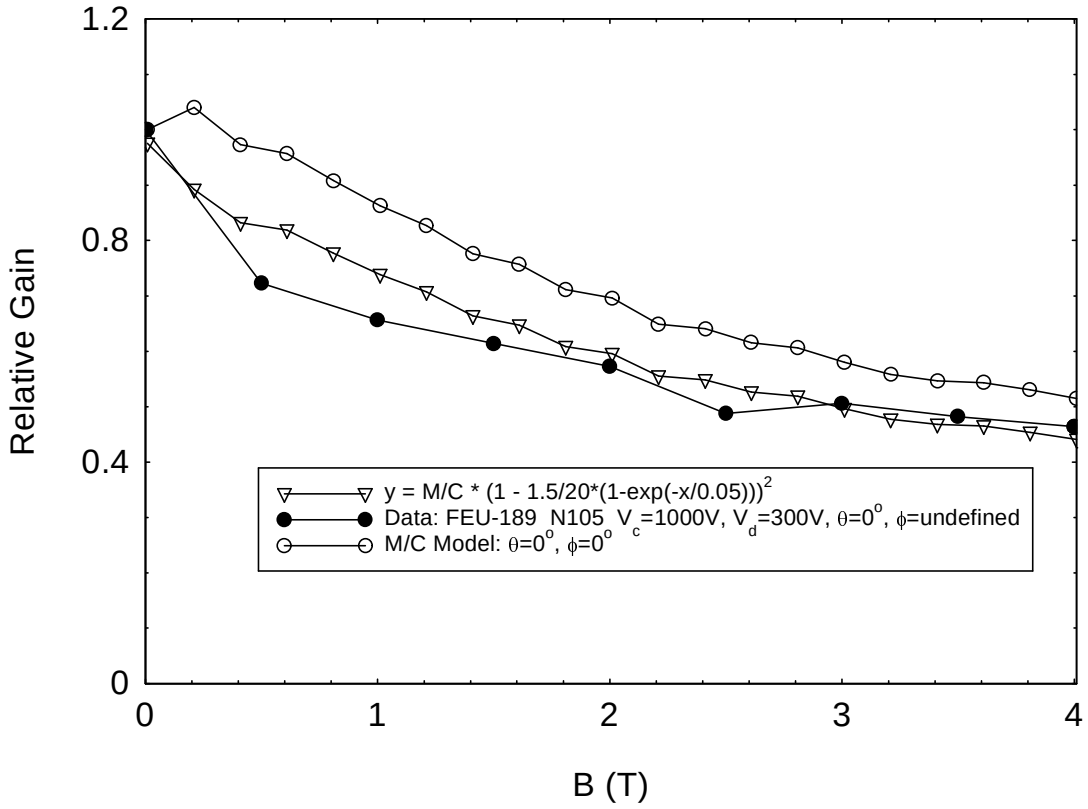

FIGURE 12

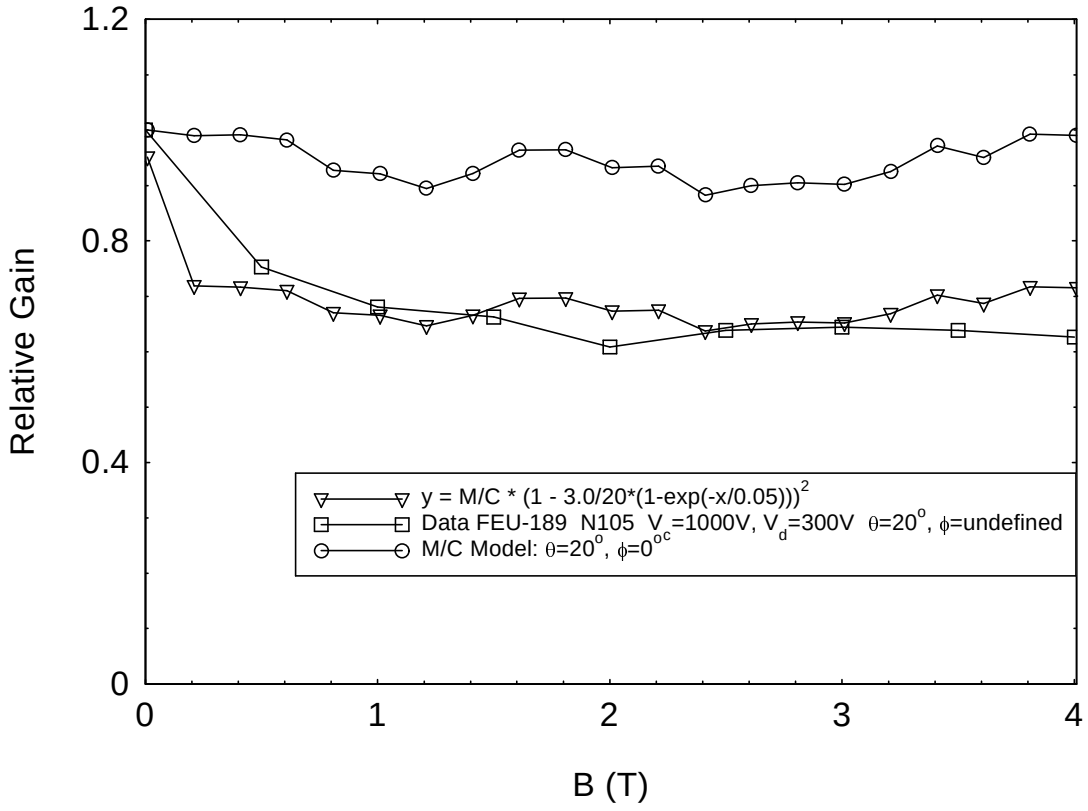

FIGURE 13

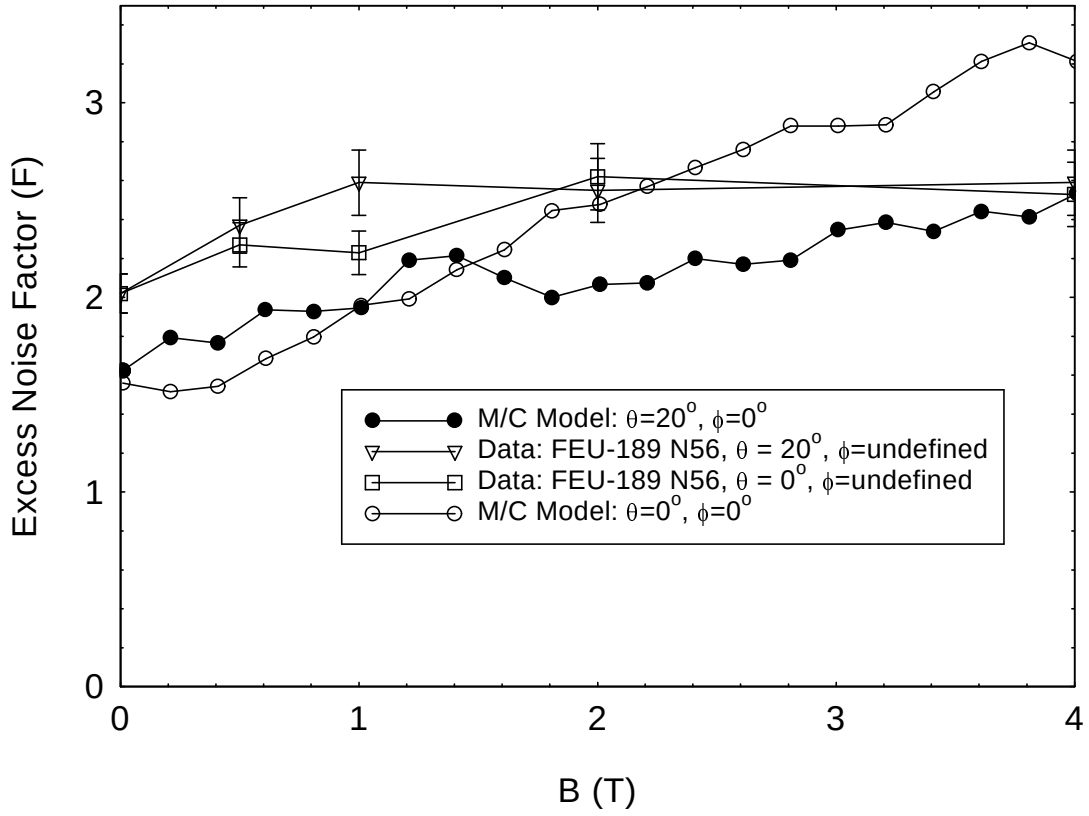

FIGURE 14

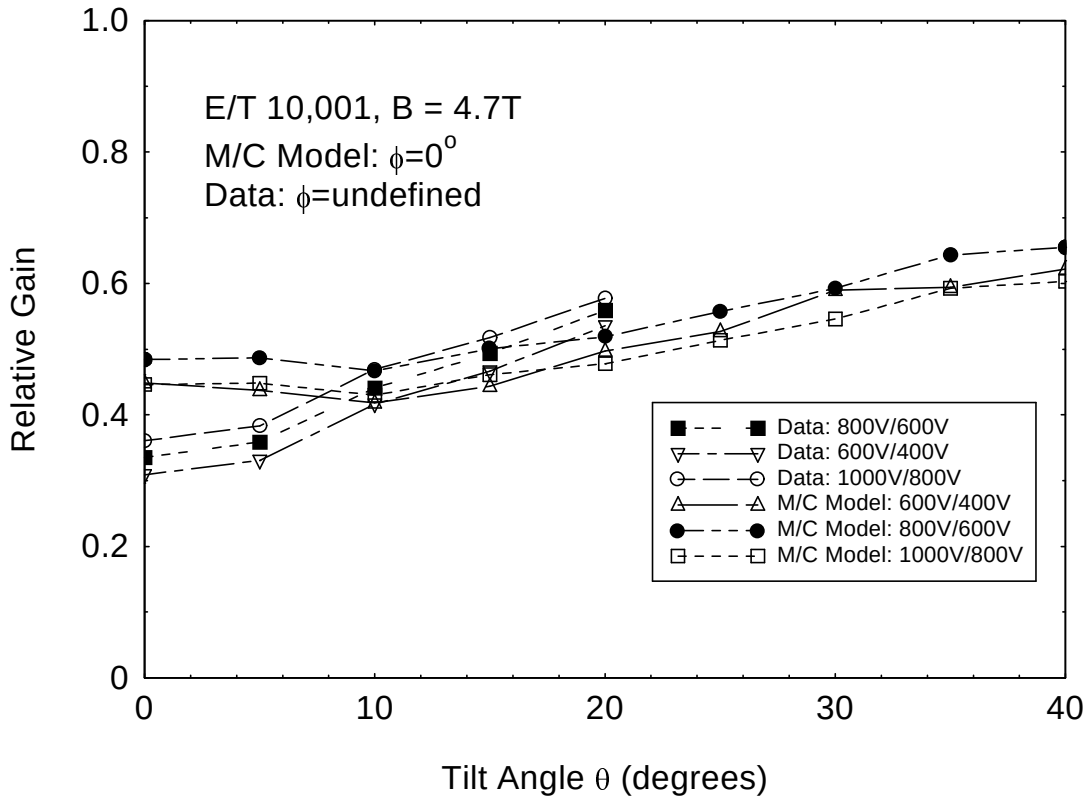

FIGURE 15

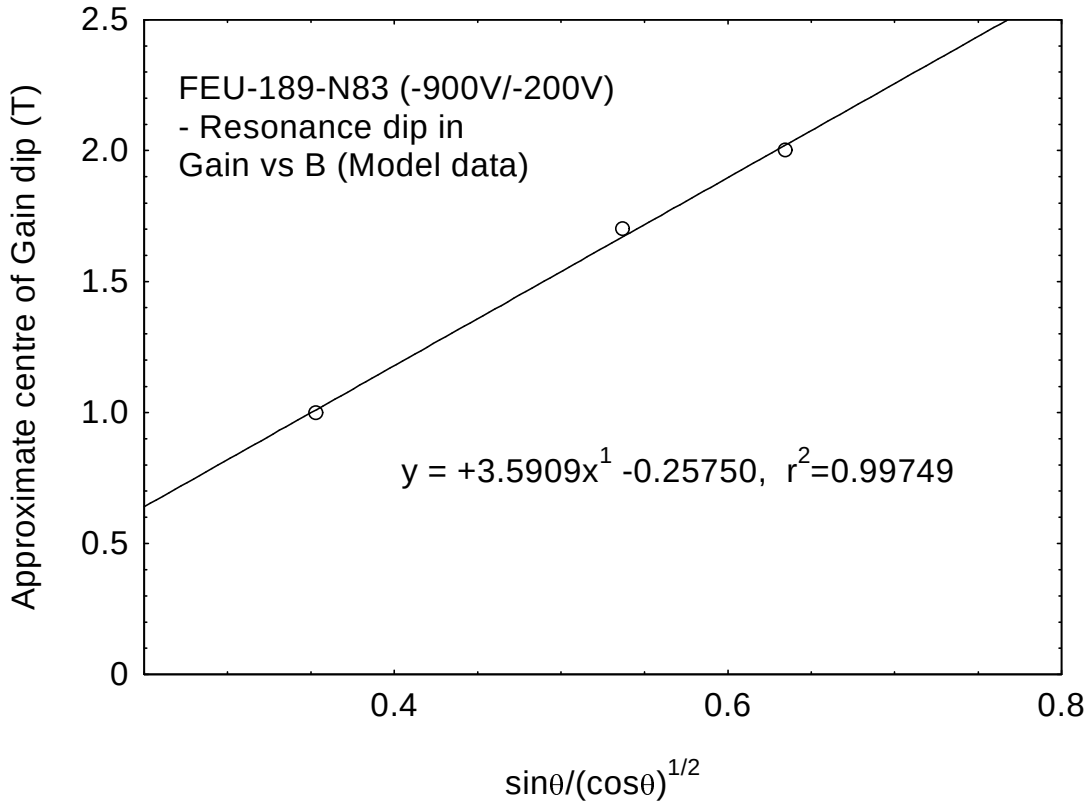
FEU-189-N83 (-900V/-200V)
- Resonance dip in
Gain vs B (Model data)
y = +3.5909x^1 -0.25750, r^2=0.99749
Approximate centre of Gain dip (T)
sinθ/(cosθ)^1/2
2.5
2.0
1.5
1.0
0.5
0
0.4
0.6
0.8